Supporting Information

A self-cleaning micro-fluidic chip biospired by the filtering system of manta rays

Xiao Hu,*[a] Longfei Yu,[a] Zuchao Zhu,[a] Fubing Bao,*[b] Jianzhong Lin,[c] Chengxu Tu[b] and Peifeng Lin[a]

a Zhejiang Key Laboratory of Multiflow and Fluid Machinery, Zhejiang Sci-Tech University, Hangzhou, Zhejiang 310018, PR China

b Zhejiang Provincial Key Laboratory of Flow Measurement Technology, China Jiliang University, Hangzhou, Zhejiang 310027, PR China

c Zhejiang Provincial Engineering Research Center for the Safety of Pressure Vessel and Pipeline, Ningbo University, Ningbo, Zhejiang 315211, PR China

Table of Contents

and the channel width is 200 μm. Dimensionless velocity profiles at the positions (E) d4 and (F) m4, and the channel width is 300 μm. The dimensionless velocity at each position in the channel is normalized using the maximum velocity under the given conditions. Dashed lines indicate the boundaries where the velocity undergoes a rapid change (w = 258 μm).

Figure S5. At an inlet flow rate of 6 mL min^{-1}, magnified plots of the dimensionless flow field velocity and pressure distribution on the $Z = 0$ cross-section, as well as the velocity and pressure distributions in the inlet and outlet sections are presented.

Figure S6. At an inlet flow rate of 8 mL min^{-1}, magnified plots of the dimensionless flow field velocity and pressure distribution on the $Z = 0$ cross-section, as well as the velocity and pressure distributions in the inlet and outlet sections are presented. The green arrow in the inserted red rectangular indicates the newly formed vortices between the filter lobes.

Figure S7. The normalized fluorescent intensity distributions of the (A) 5, (B) 15, and (C) 20 μm particles trajectories on the yellow line in Fig. 2A at different flow rates.

Figure S8. (A) Filtration efficiency for particles ranging from 10 to 20 μm in diameter when the filter lobe angle is 17°. (B) Flow rate ratio of outlet 1 for particles ranging from 10 to 20 μm in diameter at a filter lobe angle of 17°.

Figure S9. (A) Bright field image taken at the outlet section of experiment 1 (10 and 15 μm particles) at 6 mL min^{-1}. (B) Bright field image taken at the outlet section of experiment 2 (10 and 20 μm) at 6 mL min^{-1}. (C) Fluorescent stream image illustrating the particle trajectories of experiment 2 at 6 mL min^{-1}. The purple, white, and yellow arrows respectively indicate the streamlines of 10 and 15 μm particles, the streamline of 20 μm particles, and the streamline of 10 μm particles, respectively. The scale bar is 100 μm. Please note that the 20 μm particles and the 10 μm particles have the same red fluorescence. In order to clarify the equilibrium positions of the particles, arrows are used here to indicate the particle positions corresponding to their respective diameters.

Supplementary video S1. At various inlet flow rates, experiments and flow field simulations images of 10 μm particles.

Supplementary video S2. At various inlet flow rates, experimental images of 5, 10, 15, and 20 μm particles.

Table S1. When α = 13° and w = 200 μm, the summary of the inlet Reynolds number (Re_c), main channel Reynolds number (Re_m), main channel Dean number (De_m), side channel Reynolds number (Re_d) and side channel Dean number (De_d) for varying flow rates at the inlet.

Q (ml/min)	Re_c	Re_m	De_m	Re_d	De_d
0.25	32	20	1.93	12	1.19
0.5	64	40	3.87	23	2.36
0.75	96	61	5.81	35	3.54
1	128	81	7.75	47	4.72
2	255	160	15.33	95	9.61
3	383	238	22.79	145	14.64
4	510	313	29.92	198	20.01
5	638	387	37.00	251	25.44
6	766	460	44.00	306	30.94
7	893	534	51.04	360	36.41
8	1021	605	57.88	416	42.09

Table S2. When α = 17° and w = 200 μm, the summary of the inlet Reynolds number (Re_c), main channel Reynolds number (Re_m), main channel Dean number (De_m), side channel Reynolds number (Re_d) and side channel Dean number (De_d) for varying flow rates at the inlet.

Q (ml/min)	Re_c	Re_m	De_m	Re_d	De_d
0.25	32	20	2.00	12	1.23
0.5	64	40	3.98	23	2.47
0.75	96	60	5.96	35	3.71
1	128	80	7.93	47	4.98
2	255	159	15.66	97	10.16
3	383	233	23.03	149	15.73
4	510	308	30.36	203	21.35
5	638	381	37.56	257	27.10
6	766	454	44.79	312	32.82
7	893	527	52.06	366	38.51
8	1021	600	59.20	421	44.32

Table S3. When α = 21° and w = 200 μm, the summary of the inlet Reynolds number (Re_c), main channel Reynolds number (Re_m), main channel Dean number (De_m), side channel Reynolds number (Re_d) and side channel Dean number (De_d) for varying flow rates at the inlet.

Q (ml/min)	Re_c	Re_m	De_m	Re_d	De_d
0.25	32	20	2.05	12	1.27
0.5	64	40	4.10	23	2.54
0.75	96	60	6.12	35	3.84
1	128	80	8.14	47	5.15
2	255	156	15.85	99	10.75
3	383	232	23.49	151	16.44
4	510	303	30.76	207	22.52
5	638	376	38.12	262	28.51
6	766	447	45.32	318	34.65
7	893	518	52.50	375	40.84
8	1021	593	60.12	428	46.54

Table S4. When α = 13° and w = 300 μm, the summary of the inlet Reynolds number (Re_c), main channel Reynolds number (Re_m), main channel Dean number (De_m), side channel Reynolds number (Re_d) and side channel Dean number (De_d) for varying flow rates at the inlet.

Q (ml/min)	Re_c	Re_m	De_m	Re_d	De_d
0.25	23	14	1.35	9	1.01
0.5	46	27	2.72	19	2.00
0.75	69	41	4.11	28	2.97
1	92	55	5.47	37	3.97
2	184	110	10.95	74	7.92
3	276	165	16.41	112	11.90
4	369	218	21.67	151	16.09
5	461	270	26.92	190	20.29
6	553	321	31.93	232	24.76
7	645	372	37.00	273	29.16
8	737	421	41.96	316	33.67

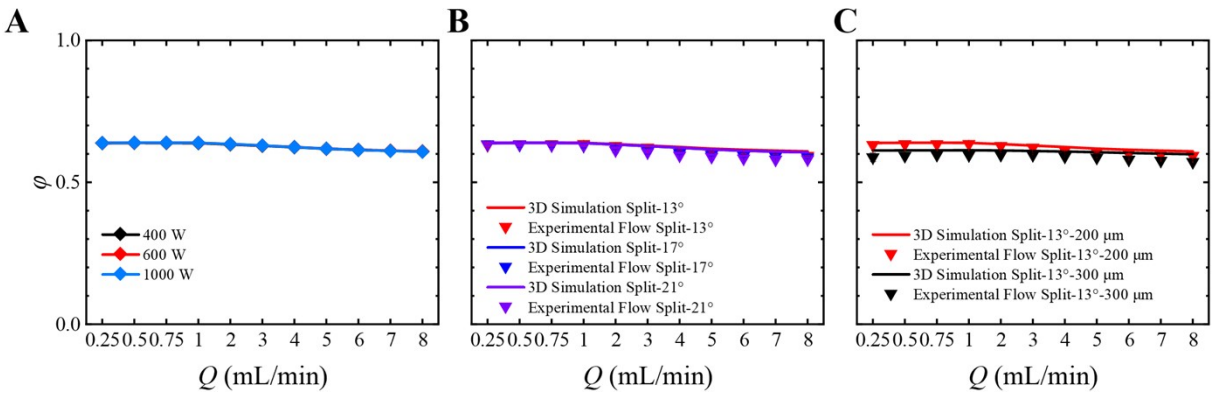

Figure S1. (A) Results for a mesh independence study monitoring outlet 1 mass flow rate. The mesh resolutions are 4 million, 6 million, and 10 million, respectively. (B) When the filter lobe angle changes, the experimental results of the flow rate ratio of outlet 1 are compared with the numerical results, revealing consistent curve trends with a relative small deviation (<5%). (C) When the channel width changes, the experimental results of the flow rate ratio of outlet 1 are compared with the simulation results, showing consistent curve trends with a relative small deviation (<5%).

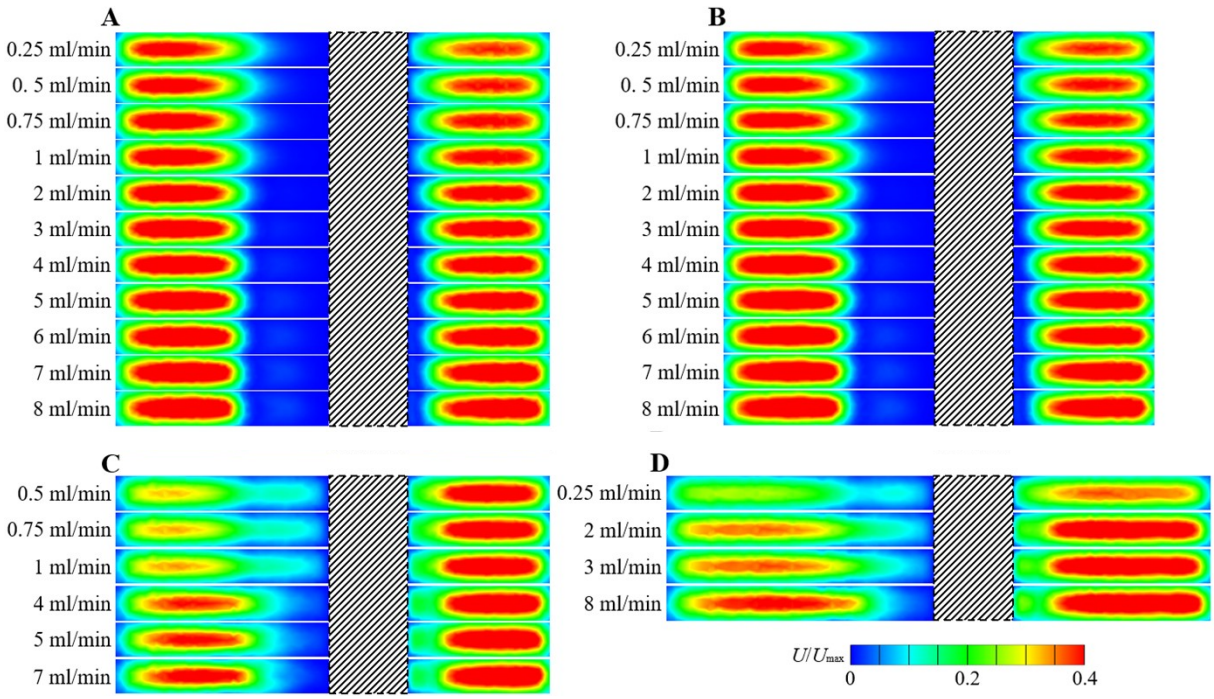

Figure S2. Simulated velocity contours along the cross-sections (A) 2, (B) 3 and (C) 4, and the channel width is 200 μm. Simulated velocity contours along the cross-sections (D) 4, and the channel width is 300 μm.

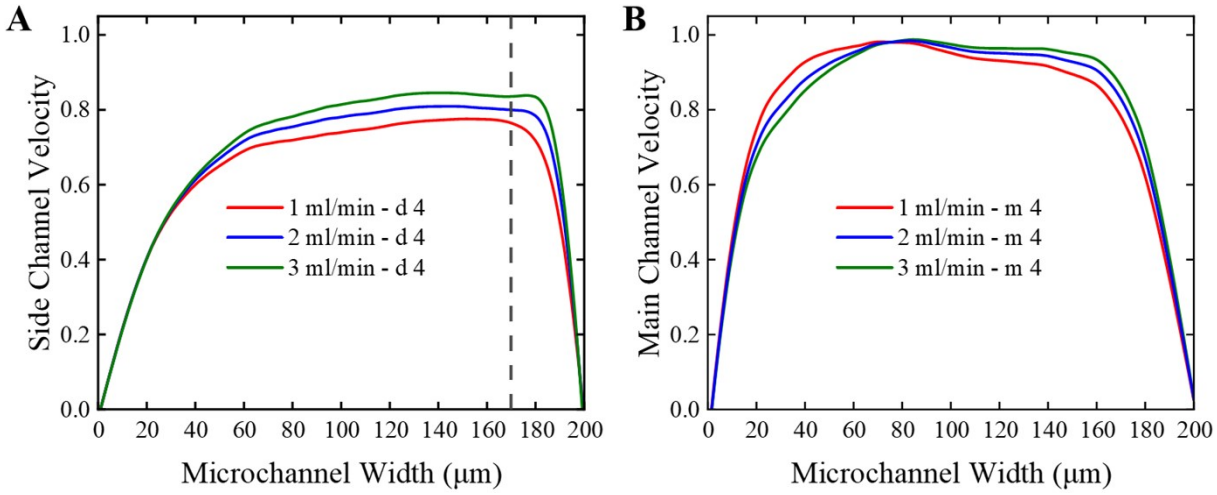

Figure S3. Dimensionless velocity profiles at the positions (A) d4 and (B) m4 for inlet flow rates of only 1, 2 and 3 ml min^{-1}. The velocity at each position in the channel is normalized using the maximum velocity under the given conditions, yielding dimensionless velocity. Dashed lines indicate the boundaries where the velocity undergoes a rapid change (w = 177 μm).

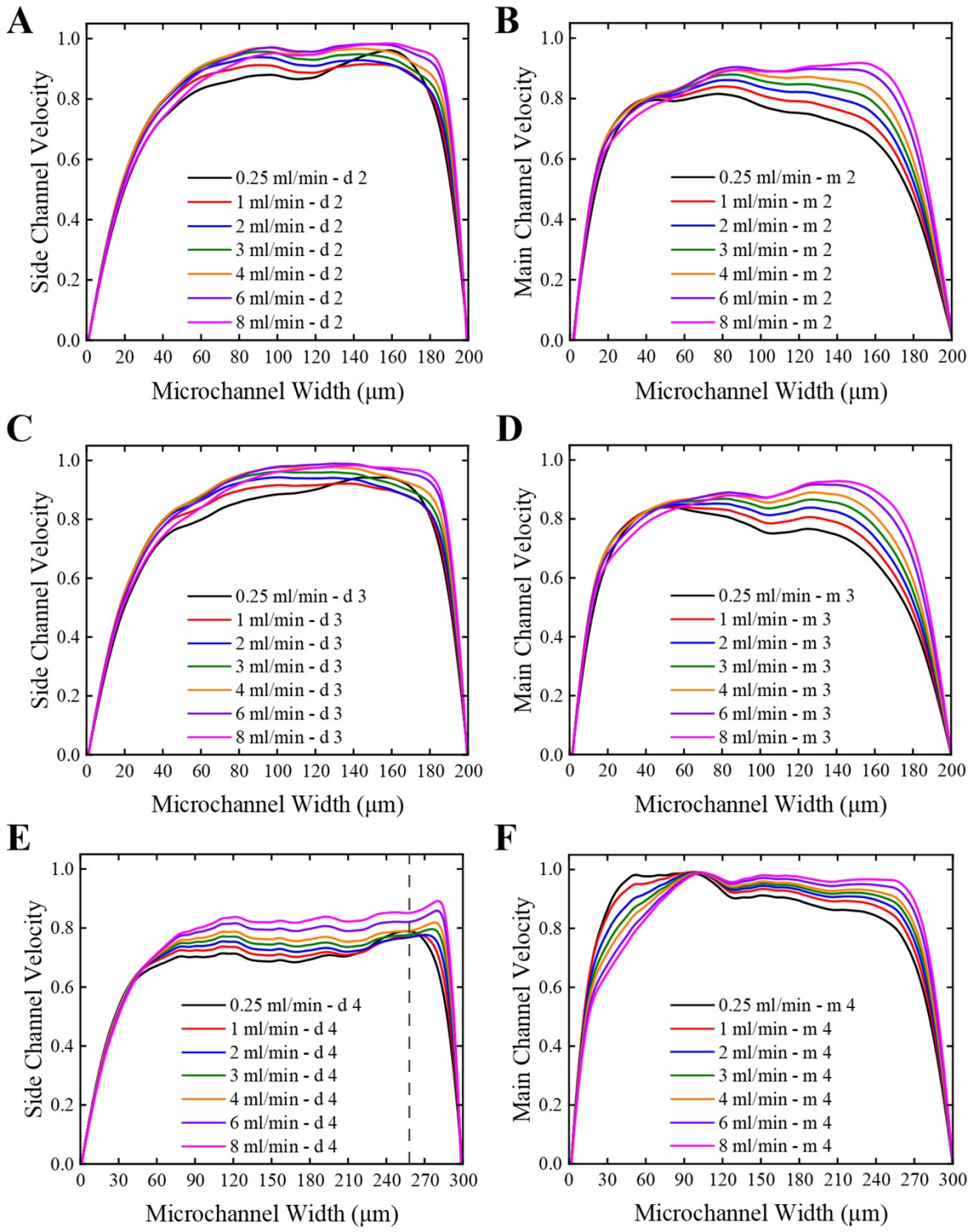

Figure S4. Dimensionless velocity profiles at the positions (A) d2, (B) m2, (C) d3 and (D) m3, and the channel width is 200 μm. Dimensionless velocity profiles at the positions (E) d4 and (F) m4, and the channel width is 300 μm. The dimensionless velocity at each position in the channel is normalized using the maximum velocity under the given conditions. Dashed lines indicate the boundaries where the velocity undergoes a rapid change (w = 258 μm).

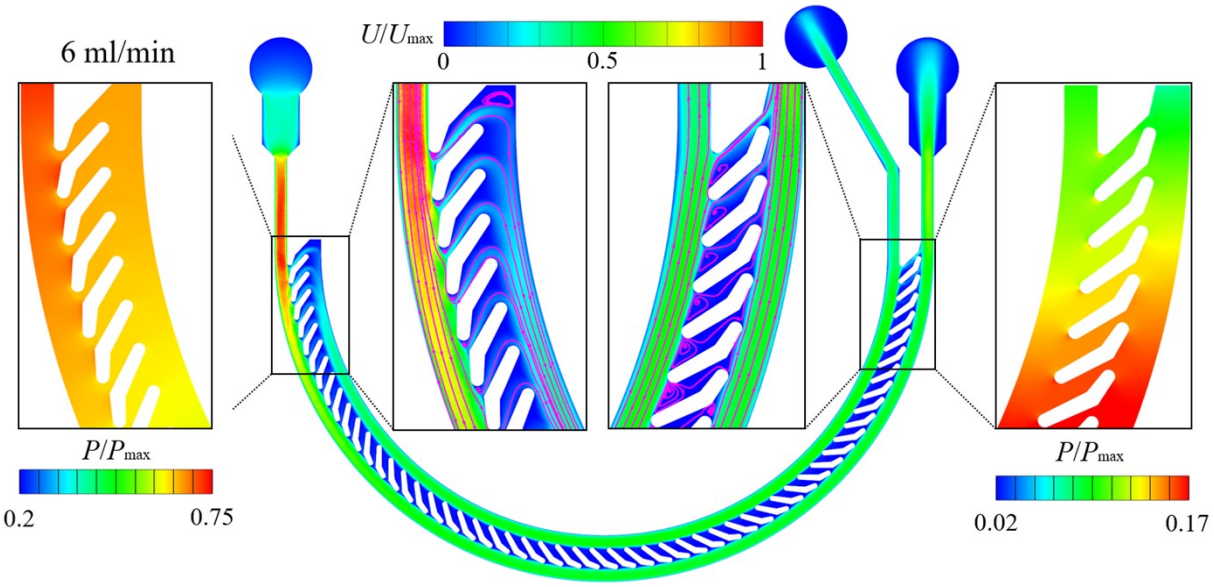

Figure S5. At an inlet flow rate of 6 mL min^{-1}, magnified plots of the dimensionless flow field velocity and pressure distribution on the $Z = 0$ cross-section, as well as the velocity and pressure distributions in the inlet and outlet sections are presented.

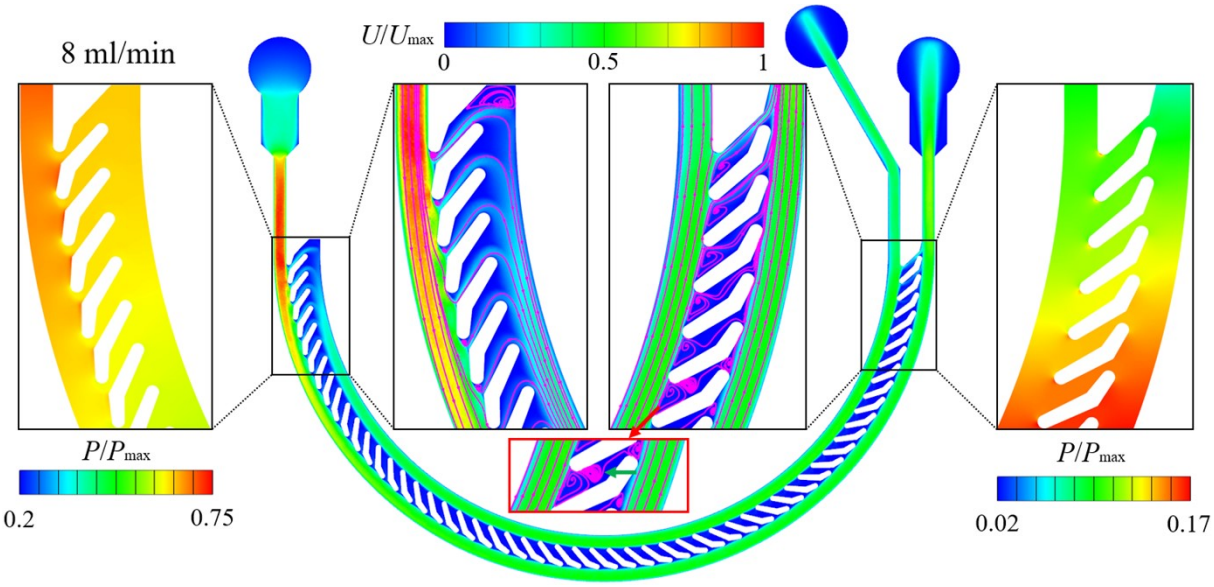

Figure S6. At an inlet flow rate of 8 mL min^{-1}, magnified plots of the dimensionless flow field velocity and pressure distribution on the $Z = 0$ cross-section, as well as the velocity and pressure distributions in the inlet and outlet sections are presented. The green arrow in the inserted red rectangular indicates the newly formed vortices between the filter lobes.

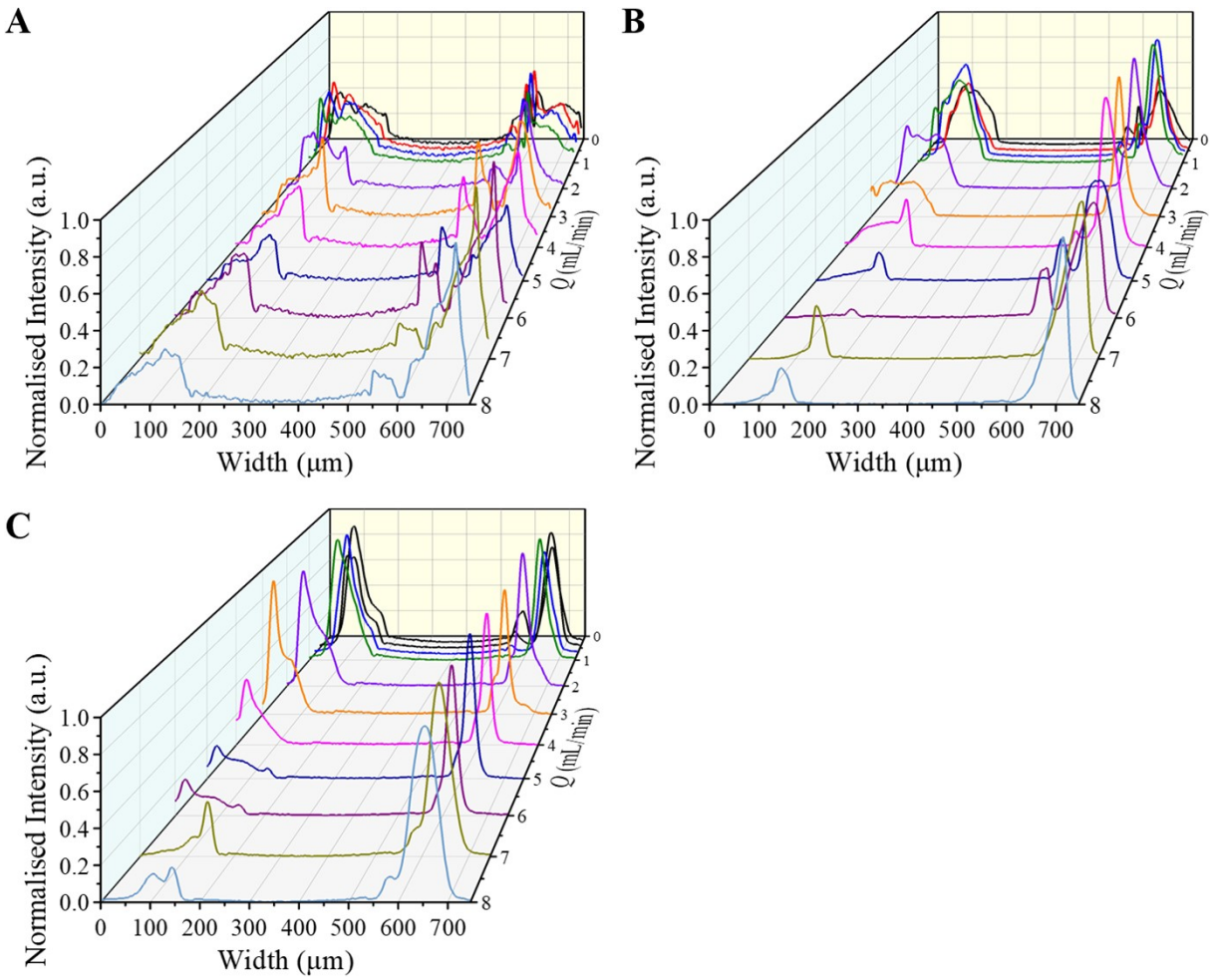

Figure S7. The normalized fluorescent intensity distributions of the (A) 5, (B) 15, and (C) 20 μm particles trajectories on the yellow line in Fig. 2A at different flow rates.

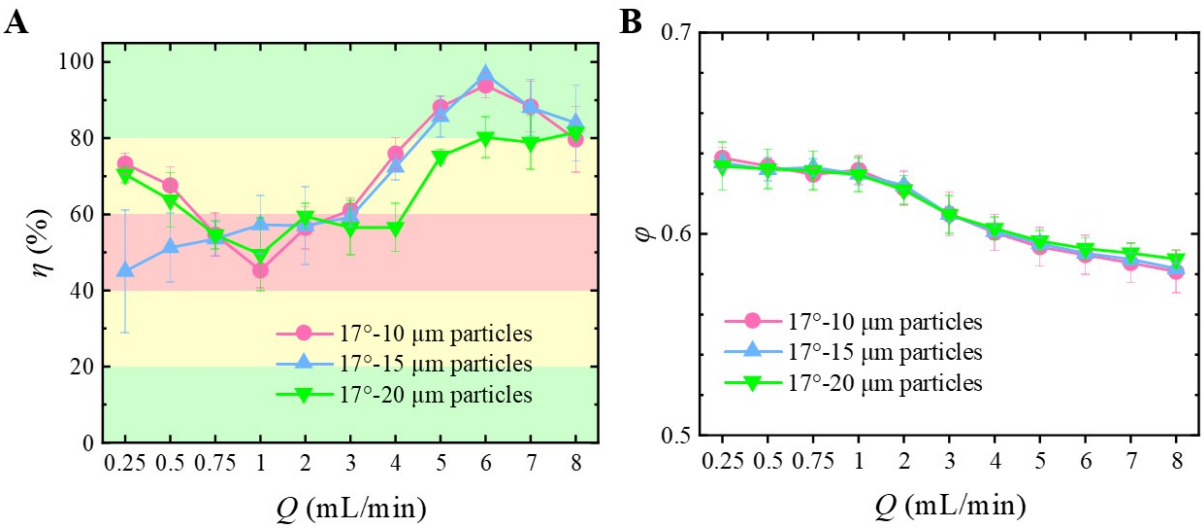

Figure S8. (A) Filtration efficiency for particles ranging from 10 to 20 μm in diameter when the filter lobe angle is 17°. (B) Flow rate ratio of outlet 1 for particles ranging from 10 to 20 μm in diameter at a filter lobe angle of 17°.

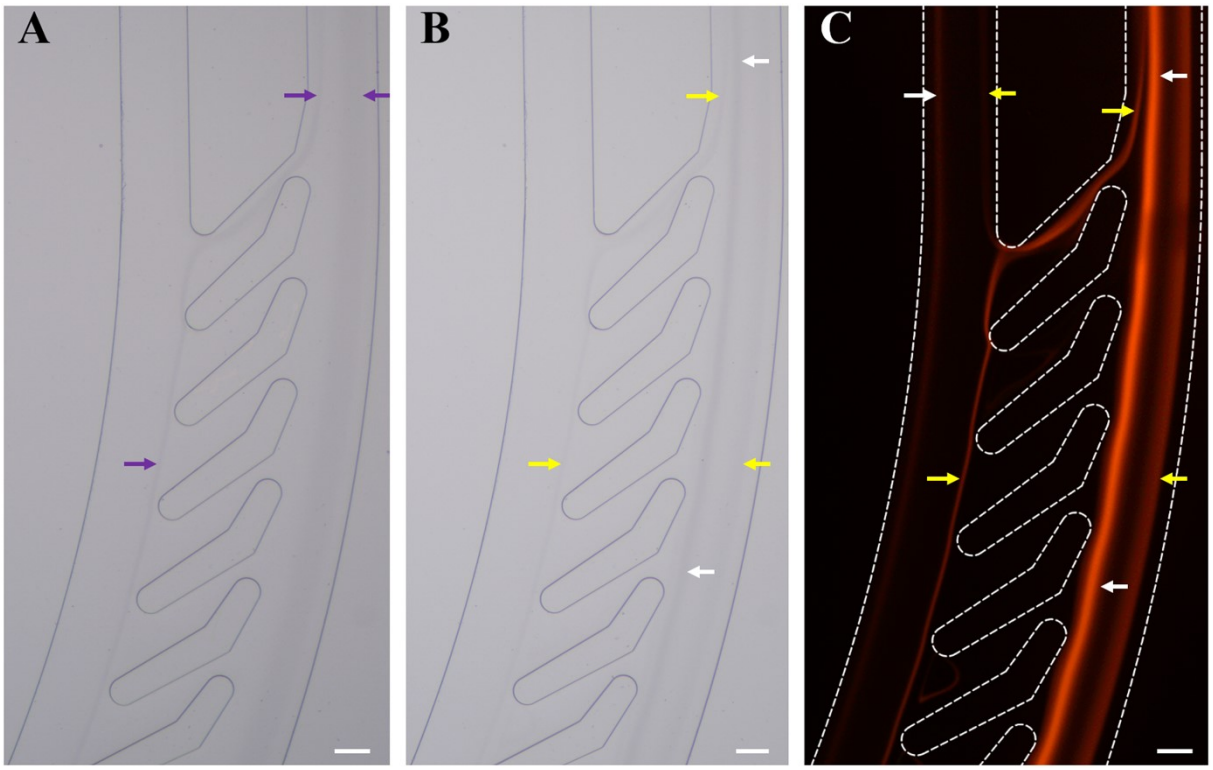

Figure S9. (A) Bright field image taken at the outlet section of experiment 1 (10 and 15 μm particles) at 6 mL min^{-1}. (B) Bright field image taken at the outlet section of experiment 2 (10 and 20 μm) at 6 mL min^{-1}. (C) Fluorescent stream image illustrating the particle trajectories of experiment 2 at 6 mL min^{-1}. The purple, white, and yellow arrows respectively indicate the streamlines of 10 and 15 μm particles, the streamline of 20 μm particles, and the streamline of 10 μm particles, respectively. The scale bar is 100 μm. Please note that the 20 μm particles and the 10 μm particles have the same red fluorescence. In order to clarify the equilibrium positions of the particles, arrows are used here to indicate the particle positions corresponding to their respective diameters.